High Pressure Falling Cylinder Viscometer - Error Analysis and Improvement Proposal

REVIEWED

Marcel Rückert*, Hubertus Murrenhoff* and Katharina Schmitz*

RWTH Aachen University, Institute for Fluid Power Drives and Systems (IFAS), Campus-Boulevard 30, D-52074 Aachen, Germany*
E-Mail: Marcel.Rueckert@ifas.rwth-aachen.de

With pressure levels rising for applications such as compression-ignition engines and numerical design approaches are used to optimise fluid power components, rheological properties of the fluid in the according operation points gain interest. The measurement of viscosity under high-pressure has been subject to research for many years. However, to this day, it still bears uncertainty. This paper presents typical errors for high-pressure measurements and strategies to minimise uncertainty. With a focus on material combinations, geometric parameters and the measurement principle, the errors are explained, and an improvement proposal is given based on the findings.

Keywords: Viscosity, Viscometer, High-pressure, Rheology, Measurement
Target audience: Tribology & Fluids, Design Process

1 Introduction

Within the cluster of excellence “Tailor-Made Fuel from Biomass” at RWTH Aachen University, alternative fuel candidates are investigated. With the increase in the people’s mobility as well as global emissions, the need for new and sustainable fuel sources is rising. To meet the increasing demand, many technological pathways are possible. With hybrid drives, electrical drives, hydrogen fuel cells and CNG-engines being researched and refined, the possibilities of alternative propulsion are already on the market. A different approach is to use the existing combustion engine infrastructure with all its components and replace the fuel with sustainable alternatives. The advantages are a clean combustion and only minor adaptions of the combustion system to these new fuels, ensuring a minor entry-barrier for this technology.

One promising candidate for usage in compression-ignition (CI) engines is di-n-butylether (DnBE). Looking at engine performance, DnBE outperforms EN 590 (Diesel) in many aspects. Especially soot emissions can be reduced drastically compared to EN 590. With injection pressures steadily rising to almost 300 MPa, fuel pumps need to be adapted to higher pressures and different fluids with hydrodynamic properties of the fluid playing a crucial role for pump performance. Figure 1 shows the dynamic viscosities of EN 590 and DnBE over pressure and temperature /1/. With a viscosity ratio of approximately six between EN 590 and DnBE, the injection pump performance using DnBE is significantly worse than for EN 590. Volumetric efficiencies reach values as low as 40 % instead of 90 % for EN 590 /2/.

The knowledge of hydrodynamic properties enables the analysis of potential improvements under consideration of the fluid. In case of the injection pump, measures can be taken to reduce solid friction by influencing the piston geometry in a way that the piston runs more concentrically. In case of volumetric losses, hollow pistons increase the volumetric efficiency up to 40% in comparison to the standard pump /3/.

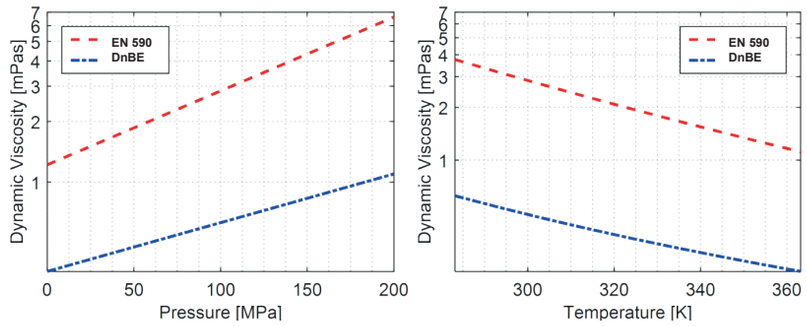

Figure 1: Pressure and temperature dependent viscosity of EN 590 and DnBE.

In hydraulics, even simple systems are heavily influenced by rheological properties. When using a standard hydraulic oil such as HLP46, a 10 K decrease in fluid temperature can change the dynamic viscosity by up to 40 %, see Figure 2 left. In a generic hydraulic resistance like a throttle, depicted in Figure 2 right, such a change in viscosity results in a differing flow rate.

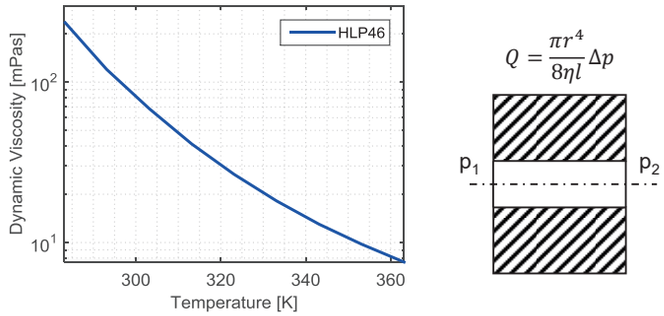

Figure 2: Temperature dependent viscosity of HLP46 (left) and fluid flow through a throttle (right).

The above-mentioned examples show the necessity to have detailed knowledge of rheological properties over temperature and pressure to design an optimal system performance. Determination of such values can be difficult, especially at high-pressure states. Viscosity measurements, for example, can be carried out using a range of principles /4/. Every principle comes with its own advantages and disadvantages. At the Institute for Fluid Power Drives and Controls (IFAS) a falling cylinder viscometer for pressures up to 300 MPa was developed /5/. Its most important advantage is the simple measurement principle. The principle is explained following.

1.1 Falling cylinder viscometers

Falling cylinder viscometers base on the principle of stokes flow. A cylinder is falling inside a fluid filled tube at low speed enabling quasistationary stokes flow with Reynolds numbers below one. The terminal velocity or the time it takes between two distinct positions is measured and can be related to the fluid viscosity if the densities of fluid and cylinder as well as the geometrical relations between tube and falling cylinder are known. Figure 3 shows the relevant parts of a falling body viscometer cell according to /5/. From the upper contact the cylinder starts falling towards the lower contact. Once it reaches the bottom position, the time is measured. In order to bring the cylinder back into initial position, a coil is positioned around the tube. By setting the voltage to a certain value, the ferromagnetic cylinder is moved up through induced magnetic forces on the cylinder. Once the cylinder reaches top position, the voltage is shut off, causing the cylinder to plummet again. One advantage of

this principle is that the measurement cell can be integrated into high pressure chambers. Only small amounts of wiring are necessary. The measurement itself works without visual sensors.

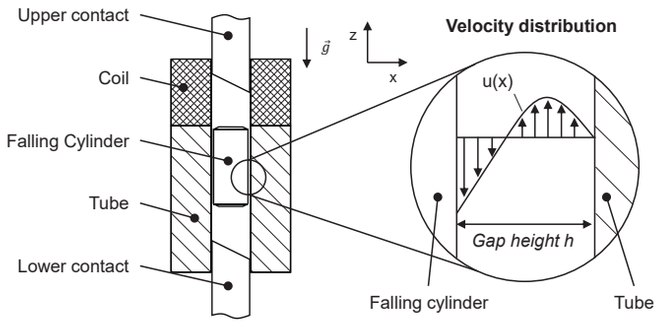

Figure 3: Principle design of a falling cylinder viscometer with essential components and flow profile in the gap between falling cylinder and tube

After each falling process, the viscosity can be calculated analytically with the densities of the fluid ρ_F and the falling cylinder ρ_{FC} as well as the falling time t_{fall}, falling distance x_{fall} and a geometry constant C, see Equation (1), which will be explained in more detail later. Especially the so-called calibration factor C and the density of the falling body can play a major role for the improvement of this measurement principle.

$$\eta = C \cdot (\rho_{FC} - \rho_F) \cdot \frac{t_{fall}}{x_{fall}} = C \cdot (\rho_{FC} - \rho_F) \cdot \frac{1}{u_{fall}} \tag{1}$$

Essential for robust viscosity measurements are reproducible falling times. Figure 4 shows the falling times over pressure for vegetable oil /6/. With increasing pressure, the falling times of the falling cylinder increase, due to higher viscosities. Ideally, these falling times move along a steady curve increasing with rising pressure and decreasing with rising temperature. Figure 4 suggests that this is hardly achieved. With deviations of 16% and more in some cases, the resulting viscosities are highly influenced by these discrepancies. Reasons for varying falling times can be found in the positioning of the falling cylinder relative to the tube. Different to the assumption of Equation (1) defining an analytical correlation of viscosity to the falling time for a cylinder positioned concentrically inside the tube, the cylinder position might be eccentric. Therefore, the resulting gap is not always uniform, and the flow cannot be calculated as easily.

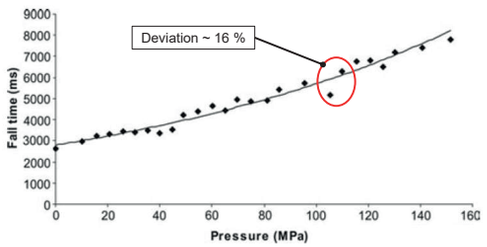

Figure 4: Falling times for a viscosity measurement with increasing pressure /6/.

For an eccentric positioning, the resulting gap height varies over the circumference of the cylinder. Using the analytical relationship for a flow through a circumferential gap with and without eccentricity, see Equation (2), the difference in falling time can be calculated using a normalised eccentricity with a maximum value of 1 /7/, see Equation (3). Figure 5 shows the falling time for normalised eccentricities of the falling cylinder inside the tube. Friction effects were neglected for this theoretical study. For increasing eccentricity values, falling times are reduced significantly and can reach theoretical values of only 40% of concentric falling times, resulting in deviating viscosities. Experiments validate these findings /8/. Using a mean for falling time scatter at constant conditions therefore does not ensure the correct time since higher values indicate a more concentric position.

$$Q = \frac{D\pi\Delta r^3}{12\eta l}\left[1 + 1.5\left(\frac{e}{\Delta r}\right)^2\right] \cdot \Delta p \tag{2}$$

$$\frac{t_{eccentric}}{t_{concentric}} = \frac{1}{\left[1 + 1.5\left(\frac{e}{\Delta r}\right)^2\right]} \tag{3}$$

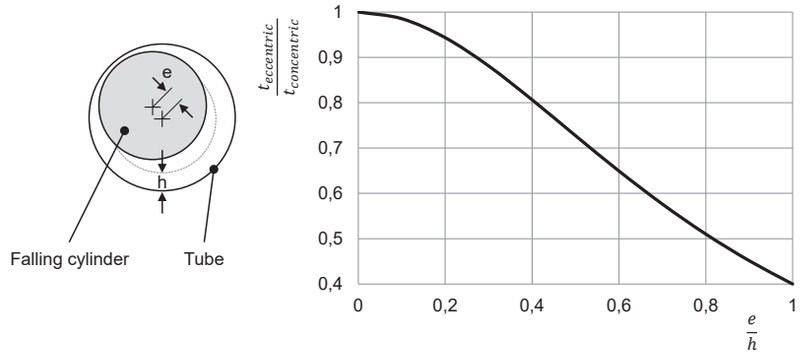

Figure 5: Falling times dependent on the eccentricity of the cylinder.

To ensure concentric alignment of falling body and tube, design changes can be made to the falling body. Here, a spherical tip is beneficial as well as a hollow end, see /7/. These changes have proven to improve the operation significantly. Nonetheless, Figure 4 shows that even with these types of sinkers, continuous falling times can hardly be achieved. Observations do show that eccentricities and tilting is still possible with adapted sinker designs. Ultimately, improvements still have to be made for an optimal design.

Ideally, the terminal velocity of the falling cylinder should be used for determination of the dynamic viscosity, see Equation (1). This would enable the detection of changes in falling behaviour due to eccentricities, tilting and other flow effects. Using a set of coils, real-time position detection based on the LVDT-principle can be realised. With a time-stamp on each position signal, a direct velocity determination is possible, enabling the evaluation of dynamic viscosities using short falling distances with higher accuracy. In order to exploit this enhanced accuracy, geometrical dependencies between tube and sinker need to be known. In the following, the highly geometry dependent calibration factor C is introduced.

1.2 Calibration factor C

Next to densities of the fluid and the falling cylinder, geometrical parameters of the tube and cylinder influence the measurement via the so-called calibration factor C. It can be derived by solving the navier-stokes equation for a cylindrical flow /9/. The analytical correlation of C with the radii of the falling cylinder (index FC) and the tube (index T) is shown in Equation (4).

$$C = \frac{1}{2} g r_{FC}^2 \cdot \left(ln\left(\frac{r_T}{r_{FC}}\right) - \frac{r_T^2 - r_{FC}^2}{r_T^2 + r_{FC}^2} \right) \tag{4}$$

In general, this constant is determined at atmospheric conditions. For a small interval of pressure and temperature, C can be viewed as constant. At high pressure or temperature conditions however, deformations significantly influence C. Deformations can be reduced by designing the viscometer in a way of limiting differential pressures of components. This has been done for the measurement cell at IFAS by placing it inside a

high-pressure chamber. Therefore, pressure forces act on tube and cylinder both from the in- and outside of the tube.

2 Application oriented material selection

Increasing pressure levels of diesel injection systems up to 300 MPa required an adaption of the viscometer towards higher pressures. The test-rig was upgraded for pressures up to 750 MPa and temperatures between 253.15 K and 353.15 K. These conditions can cause significant deformations of cylinder and tube. Therefore, suitable material selections based on the operating conditions of the test-rig are necessary. Due to the usage of the LVDT-principle, the falling body has to be made of ferromagnetic material whereas the tube has to be non-magnetic. In the following, three different material-pairings are investigated, see Table 1.

Pairing No.	Falling cylinder	Tube
1	S355-steel	CuZn37 - brass
2	CuZn37 – brass (ferromagnetic)	CuZn37 - brass
3	S355-steel	X5CrNi18-10 – 1.4301

Table 1: Investigated material pairings for the falling body viscometer.

In general, materials with good thermal and mechanical stress-resistance are suited for usage within the pressure cell. Limiting factor is the ability of the materials for mechanical treatment and achievable tolerances. The pairings chosen display good properties for all aforementioned aspects or have been used in other applications, see /10/.

With FEM analysis pressure- and temperature-dependent deformations can be calculated. Figure 6 shows the resulting deformations of tube and cylinder as well as the effective gap change over pressure and temperature for the first material pairing. Negative values indicate a shrinking while positive values signal expansion. For the first material pairing, the tube changes its geometrical shape with higher gradients than the cylinder resulting in an overall change in gap-height with values of up to -5.793 µm for 253.15 K and 800 MPa and 5.479 µm for 353.15 K and 0 MPa.

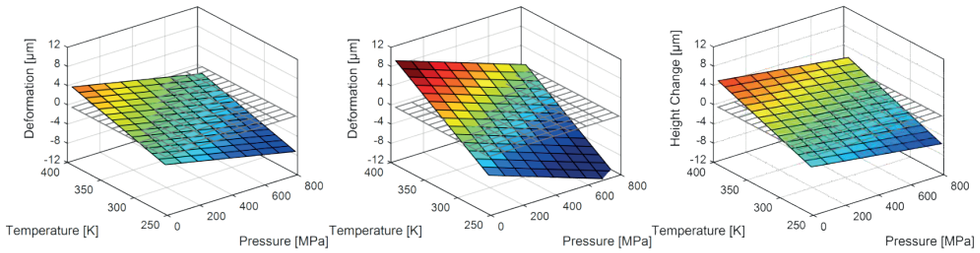

Figure 6: Deformation array over pressure and temperature for cylinder (S355-steel, left), tube (brass, middle) and resulting gap change (right).

The resulting gap height for pairings no. 2 and 3 are shown in Figure 7. Both graphs indicate a significant improvement compared to the S355-brass-pairing. Both pairings show less change over temperature and pressure. Overall results with the maximum deformations can be found in Table 2. Here, the error displays the relative change in gap height compared to ambient conditions. Pairing 1 shows deviations in temperature (T) and pressure (p) domain of up to 15.5 %. For pairing 2 and 3 those values are around 10 % with pairing 2 performing better over temperature and pairing 3 showing advantages during pressure dominant operation.

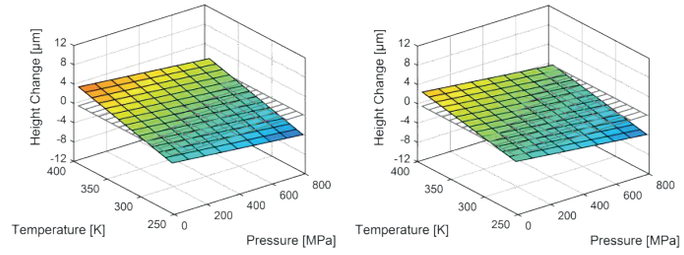

Figure 7: Change in gap height for pairing 3 (left) and pairing 2 (right).

Pairing No.	Radius dev. - Cylinder [µm]	Radius dev. - Tube [µm]	Resulting Gap height change [µm]	Max. error (T) [%]	Max. error (p) [%]
1	-7.37 / 4.258	-13.16 / 9.74	-5.79 / 5.48	15.41 %	13.34 %
2	-13.16 / 9.74	-9.12 / 6.78	-4.04 / 2.96	8.67 %	10.63 %
3	-7.37 / 4.26	-11.52 / 8.2	-4.15 / 3.95	11.41 %	9.67 %

Table 2: Deformation results for all material pairings: Minimum and maximum values as well as the maximum error values for pressure- and temperature-dependent deformations.

Using the information of deformation over pressure and temperature, the C-factor can be determined for every pairing in every possible measurement condition, see Figure 8. Thus, the pressure and temperature dependency can be visualised. A lower gradient indicates a more constant value over the domain. For a constant C-factor over temperature and pressure, a pairing has to be found, that has optimal thermal and mechanical behaviour. If the S355-stell falling body is selected, the tube has to have a bulk modulus of around 70 % of S355-steel to provide constant values over pressure. As for temperature, the thermal expansion coefficient needs to be around 50 % of the value of S355-steel. In addition, the potential material needs to be non-magnetic in order to not influence the position measurement of the falling body. A material pairing enabling a temperature and pressure independent calibration factor has not yet been found .

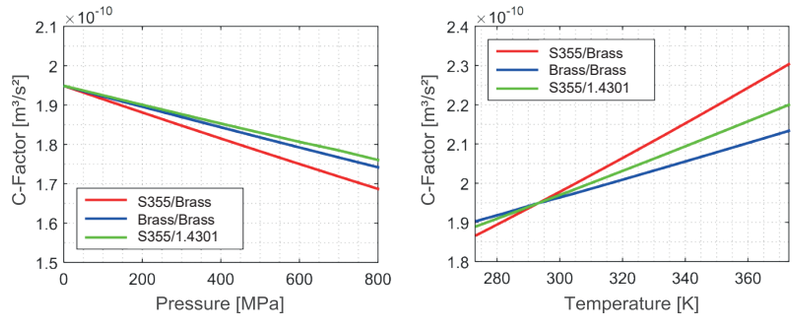

Figure 8: C-factors for pairings 1 to 3 over pressure (@ 293.15 K) and temperature (@ 0 MPa).

3 Improvement towards more robust measurements

According to Equation (1) viscosity measurements based on the falling body principle always need information of the fluids density at the investigated conditions. To minimise measurement errors, the density must be determined simultaneously with the viscosity measurement in one pressure cell. This is not possible, when the cell requires disassembling for integrating different measurement devices. As a solution a novel approach was proposed /11/. Here, two different falling bodies are used within the same tube, causing two different falling speeds. If both bodies do fall within the stokes flow regime, the viscosity and the density can be determined simultaneously. With the bodies 1 and 2 falling with two different speeds, two equations with two unknowns result. Therefore, density can be substituted by the geometry and velocity of the other falling body, see Equation (5) to (7).

$$\eta = C_1 \cdot \left(\rho_{FC_1} - \rho_F\right) \cdot \frac{1}{u_1} = C_2 \cdot \left(\rho_{FC_2} - \rho_F\right) \cdot \frac{1}{u_2} \tag{5}$$

$$\rho_F = \frac{C_1 \rho_{FC_1} u_2 - C_2 \rho_{FC_2} u_1}{C_1 u_2 - C_2 u_1} \tag{6}$$

$$\eta = \frac{C_1 C_2 \rho_{FC_1} - C_1 C_2 \rho_{FC_2}}{C_1 u_2 - C_2 u_1} \tag{7}$$

With current viscometer designs, it is only possible to use one falling body inside a tube. Therefore, a disassembly of the pressure cell is necessary in order to exchange falling bodies. This results in different conditions as well. To reduce the measurement error, a new viscometer design is proposed. Figure 9 shows this design. A cascade of coils that can be actuated individually, initially keeps both bodies at the top of the tube. With individual control of each coil, it is possible to cause body 2 to fall while body 1 is still at the top position. Once body 2 arrives at the bottom of the tube, the falling process for body 1 is initiated. This way, both bodies are not influencing each other during the fall. For this principle to work, the tube length has to be sufficient for two falling bodies within the measurement device. If the aforementioned criteria are met, an in-situ measurement of density and viscosity is possible, reducing measurement error and enhancing reliability of the data.

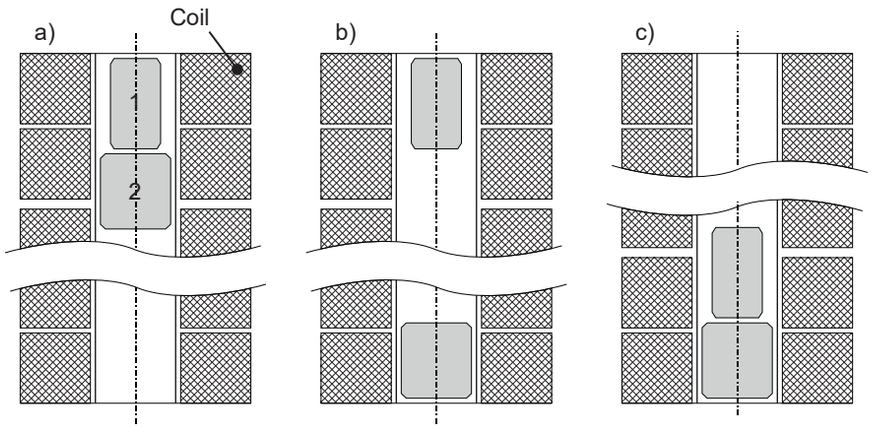

Figure 9: Improved viscometer principle: Both falling bodies at initial position (left), body 2 at the bottom (middle) and after a complete measurement (right).

4 Summary and Conclusion

In this paper, an error analysis of falling body viscometers was carried out considering material pairings and resulting pressure- and temperature-dependent deformations as well as the measurement principle. Falling body viscometers enable viscosity measurement at high pressures and temperatures since they do not rely on optical sensors. Based on the LVDT-principle, determination of the terminal velocity is possible, enhancing the measurement accuracy. To further increase measurement precision, material pairings of tube and body can be found that cause a favourable performance regarding the deformation under pressure and temperature. In addition, regarding errors caused by material deformations, a sequential falling process with two geometrically similar falling bodies of different was proposed, enabling in-situ viscosity and density measurements.

With the knowledge of material behaviour, measurement devices can be designed with regard to planned operation conditions. Combining the knowledge of material pairings with an improved viscometer design, the measurement accuracy can be increased significantly, providing more reliable rheological data for simulations and the design of fluid power applications.

To realise this potential, a new measurement device has to be developed. Additionally, suited material pairings have to be investigated in regards of achievable manufacturing tolerances.

5 Acknowledgements

This work was performed as part of the Cluster of Excellence "Tailor-Made Fuels from Biomass", which is funded by the Excellence Initiative by the German federal and state governments to promote science and research at German universities.

Nomenclature

Abbreviation	***Description***
CI	*Compression-ignition*
CNG	*Compressed natural gas*
DnBE	*Di-n-Butylether*
EN 590	*Diesel fuel*
HLP	*Mineral based hydraulic oil with corrosion and high-pressure additives*
IFAS	*Institute for fluid power drives and controls*
LVDT	*Linear variable differential transformer*

Variable	***Description***	***Unit***
C	Calibration factor	[m³/s²]
D	Diameter	[m]
e	Eccentricity	[m]
g	Gravitational acceleration	[m/s²]
h	Height	[m]
l	Length	[m]
p	Pressure	[Pa]

Q	Flow rate	[m³/s]
r	Radius	[m]
T	Temperature	[K]
t	Time	[s]
u	Velocity	[m/s]
x	x-direction	[m]
z	z-direction	[m]
η	Dynamic viscosity	[Pas]
ρ	Density	[kg/m³]

Index	***Description***
1	*Body/position no. 1*
2	*Body/position no. 2*
$concentric$	*Concentric alignment*
$eccentric$	*Eccentric alignment*
F	*Fluid*
FC	*Falling cylinder*
$fall$	*During the falling process*
T	*Tube*

References

/1/ Weinebeck, A., et al., "*Tribological Investigations of new biofuel blends*", 19th International Colloquium Tribology, Technische Akademie Esslingen, Tribology - industrial and automotive lubrication, Stuttgart/Ostfildern, Germany, 2014.

/2/ Heitzig, S., "*Analyse und Optimierung biokraftstoffgeschmierter Tribosysteme in Common-Rail-Pumpen*", Dissertation, Shaker Verlag, Aachen, Germany, 2016.

/3/ Rückert, M., et al., "*Influence of a new hollow piston design on volumetric losses of a common-rail pump*", Proceedings of the ASME/BATH 2017 Symposium on Fluid Power and Motion Control, FPMC2017-4231, Sarasota, USA, 2017.

/4/ Assael, M.J., et al., "*Experimental Thermodynamics Volume IX - Advances in Transport Properties of Fluids - Chapter 4 – Viscometers*", Royal Society of Chemistry, UK, 2014.

/5/ Drumm, S., "*Entwicklung von Messmethoden hydraulischer Kraftstoffeigenschaften unter Hochdruck*", Dissertation, Shaker Verlag, Aachen, Germany, 2012.

/6/ Schaschke, C.J., et. al., „Viscosity measurement of vegetable oil at high pressure", Trans IChemE, Part C, Food and Bioproducts Processing, 84(C3): 173-178, 2006.

/7/ Murrenhoff, H., *"Fundamentals of Fluid Power"*, Lecture notes, RWTH Aachen, 2014.

/8/ Irving, J. B., "*The effect of nonvertical alignment on the performance of a falling-cylinder viscometer*", Journal of Physics D: Applied Physics, Vol.5, 1972.

/9/ Cristescu, N.D. et. al., "*A closed form solution for falling cylinder viscometers*", International Journal of Engineering Science 40 (2002) 605-620, 2002.

/10/ Blume, J., "*Druck- und Temperatureinfluss auf Viskosität und Kompressibilität von flüssigen Schmierstoffen*", Dissertation, RWTH Aachen, Aachen, Germany, 1987.

/11/ Zeng, M., Schaschke, C., „*High Pressure Falling Sinker Liquid Viscosity Determination without Supplementary Density Data: A New Approach"*, International Journal of Chemical Engineering, 2009.